Robotica (2018) volume 36, pp. 1436–1453. © Cambridge University Press 2018
doi:10.1017/S0263574718000486

An unmanned helicopter control with partial small body force compensation: Experimental results

Bryan Godbolt† and Alan F. Lynch‡*

†*QinetiQ Target Systems, Medicine Hat, AB, Canada. E-mail: bryan.godbolt@qinetiq.ca*
‡*Department of Electrical and Computer Engineering, University of Alberta, Edmonton, AB, Canada*

(Accepted May 25, 2018. First published online: July 3, 2018)

SUMMARY
A generally accepted helicopter model used for control includes the effect of Small Body Forces (SBF) which couple the vehicle's rotational subsystem inputs to its translational dynamics. SBF result from tail rotor thrust and lateral forces due to main rotor flapping. It is well-known that SBF lead to a theoretically challenging stabilization problem for the tracking error dynamics. Hence, much of the existing work has neglected SBF in order to simplify control design. We design a controller that directly compensates the influence of the tail rotor component of the SBF. The design is validated in simulation and flight tests.

KEYWORDS: Aerial Robotics; Control of Robotic Systems; Robot Dynamics; Mechatronic Systems; Automation.

1. Introduction

Motion control of unmanned conventional helicopters is currently an active topic of research. A *conventional* helicopter is a rotary-wing aircraft with a tail and main rotor as shown in Fig. 1. The larger main rotor blades rotate about the vehicle's vertical axis and provide thrust which is controlled by a collective pitch input. The smaller tail rotor blades rotate in a vertical plane about the vehicle's lateral axis. Tail thrust is controlled by a collective pitch input and serves to counter the reaction torque of the main rotor and control yaw motion. This rotor configuration is commonly found on manned helicopters and provides unique translational motion control including hover, and vertical takeoff and landing (VTOL). The helicopter's special manoeuvrability has established its use in applications such as surveillance, cargo transportation, and inspection of infrastructure. Control of translational motion is achieved by orienting the vehicle and main rotor thrust. Roll and pitch motion control is obtained by main rotor flapping which is related to cyclic pitch inputs. The literature on model-based control of small unmanned helicopters is based on a number of different models. Different simplifications are used to obtain low-dimensional models which make control design tractable. For example, many authors use linear model approximations so that linear control design methods can be applied.[3,7,29] On the other hand, this paper adopts a nonlinear model similar to that presented in refs. [8, 24, 26]. A key aspect of the model is the coupling due to rotational subsystem inputs which appear in the translational dynamics. These coupling forces are commonly referred to as *Small Body Forces (SBF)*.[18,24,26] The partial compensation of SBF and the analysis of the remaining components is the main contribution of this paper. SBF arise in part from main rotor flapping which is described by two flapping angles parameterizing the relative orientation of the main rotor disk to the airframe. Tail rotor thrust also contributes to SBF since it creates a horizontal force and affects lateral motion. For example, since the tail rotor is used to control heading during hover it creates a steady-state disturbance to the translational dynamics. In general, since the tail rotor must generate significant thrust to balance or overcome the main rotor countertorque (e.g., for yaw motion), this disturbance thrust is expected to dominate other forces such as fuselage drag. The SBF coupling makes the theory of control design challenging. For

* Corresponding author. E-mail: alan.lynch@ualberta.ca

https://doi.org/10.1017/S0263574718000486 Published online by Cambridge University Press

example, work in ref. [24] shows SBF result in unstable internal dynamics (i.e., a nonminimum phase system) which prevents input–output linearization. It is therefore common practice to neglect SBF in the control design, e.g., refs. [8, 27, 28, 36]. In ref. [26], the SBF are neglected to derive a control, and their effect on tracking error performance is analyzed as a disturbance. Ultimate boundedness of the trajectory tracking error is proven. A similar analysis for approximate input–output linearization is obtained in ref. [24]. Although there are a number of challenges involved in helicopter control (e.g., uncertainty due to complex blade aerodynamics), compensation of SBF is an established and important problem in the literature. The contribution of this paper is to derive a control law which *compensates* the tail rotor component of the SBF, and to analyze the stability of the remaining SBF components due to rotor flapping. A preliminary version of this work was presented in ref. [11]. However, unlike that work, we present experimental validation of the control law which is normally absent in the literature.[24,26] Experimental validation is crucial to ensure a control law can be implemented on-board the autopilot and be robust to the inevitable modelling assumptions required to make control design tractable (e.g., unmodelled wind gust disturbance or aerodynamics modelling). The paper also presents simulation results which have been optimized to show why SBF compensation improves tracking error relative to the industry-standard inner-outer loop PID (proportional-integral-derivative) control structure. Further, additional details are provided for the control design and the proof of robustness. It is important to note that the robustness analysis leads to a specific statement about the performance trade-offs of the proposed design.

Recently, other types of unmanned rotary-wing vehicles have received tremendous attention in the literature.[39] In particular, multirotors are popular due to their simple, inexpensive, and robust construction. Although modelling of multirotors often neglects propeller flapping (e.g., ref. [41]), recent work[30] includes its effect to improve model-based motion control. Here, as with conventional helicopters, blade flapping leads to a disturbance term in the translational dynamics. However, since the term is linear velocity dependent as opposed to depending on rotational subsystem inputs, this disturbance is therefore not a SBF, and its compensation less challenging.[30] It is interesting to note that SBF exist in tandem rotor configured helicopters[8] and in ducted fan tailsitters.[17]

There is a significant amount of existing research on robust nonlinear control for helicopter and multirotor UAVs. This work does not focus on SBF in particular but rather consider a more general case of disturbance torque entering the rotational dynamics and disturbance force entering the translational dynamics. These disturbances are intended to model a broad range of uncertainty such as wind forces. Many of such robust nonlinear controls are based on backstepping[4] which is combined with disturbance observers[15,37] or adaptive control[6] to improve the attenuation of disturbances. Since the problem considered in these papers is more general, the resulting control laws are more complex than the one proposed here and do not provide better convergence properties.

Section 2 summarizes the model of the helicopter and establishes notation. In Section 3, the proposed control is presented and is performed in two steps. This common approach is similar to work in refs. [7, 20, 40]. The idea is to treat the rotational subsystem as an actuator for the translational dynamics. In addition to the advantage that the underactuated system becomes two fully-actuated systems in cascade, this approach also provides the benefit that the outer-loop dynamics can be analyzed using known expressions for the inner-loop inputs. This benefit is the basis of our approach. The inner-loop control is presented first and stabilizes the rotational dynamics. The reference trajectory for this inner-loop is provided by an outer-loop design for the translational dynamics. The inner-outer loop approach is also used in[28] for helicopters and[21] for quadrotors as well as many other references. In fact, the inner-outer loop structure is found in most autopilots which have been extensively field tested.[34] Since our approach does not compensate the SBF associated with the main rotor flapping, we analyze their effect on the closed-loop stability in Section 4, and show that the system remains uniformly ultimately bounded. Simulation results are presented in Section 5, comparing the design with PID control. Experimental results and a description of the platform is given in Section 6.

2. Modelling

Consider two coordinate frames $\mathcal{N}$ and $\mathcal{B}$ whose axes are aligned with the orthogonal unit vectors $\{e_1, e_2, e_3\}$ and $\{e'_1, e'_2, e'_3\}$, respectively. The navigation frame $\mathcal{N}$ is assumed inertial, has its origin fixed to the surface of the earth, and has its axes oriented north, east, and down. The body frame $\mathcal{B}$ is attached to the helicopter's centre of mass; and its axes pointing forward, right, and down. Figure 1

https://doi.org/10.1017/S0263574718000486 Published online by Cambridge University Press

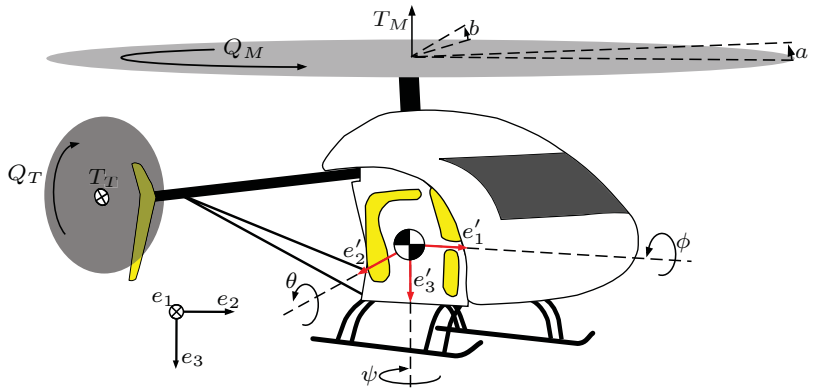


Fig. 1. Notation and reference frames used in the helicopter modelling.

shows the reference frames and notation used in the helicopter modelling. See ref. [9] for further details on the various coordinate frames used for navigation. The dynamics of the helicopter can be described using the Newton–Euler equations for a rigid body

$$\dot{p}^n = v^n \tag{1a}$$

$$m\dot{v}^n = mge_3 + f \tag{1b}$$

$$\dot{R} = R\hat{\omega} \tag{1c}$$

$$J\dot{\omega} = -\omega \times J\omega + \tau, \tag{1d}$$

where p^n, $v^n \in \mathbb{R}^3$ are position and velocity in $\mathcal{N}$; m, J are mass and inertia; g is acceleration due to gravity; $R \in SO(3)$ is the rotation matrix that represents orientation; $\omega \in \mathbb{R}^3$ is angular velocity in $\mathcal{B}$; and f, $\tau \in \mathbb{R}^3$ are applied force and torque in $\mathcal{N}$ and $\mathcal{B}$, respectively. The superscript in p^n refers to coordinates being defined in the navigation frame. The map $\hat{\cdot} : \mathbb{R}^3 \to so(3)$ is an isomorphism between 3-vectors and 3×3 skew-symmetric matrices, and its inverse is denoted $(\cdot)^\vee : so(3) \to \mathbb{R}^3$. Although several parameterizations of the rotation matrix are commonly used,[38] we will make use of the Euler angle roll-pitch-yaw parameterization, denoted ϕ, θ, ψ, respectively. In addition, we will use the notation $R = R_z R_y R_x$ for this parameterization.

A commonly accepted model for the applied force f and torque τ is presented in several references (e.g., refs. [8, 24]). In addition, detailed treatments of the aerodynamic modelling can be found in e.g., refs. [2, 19, 25, 29, 31, 33]. We summarize the model here in order to establish notation. The applied force is

$$f = R \begin{pmatrix} -T_M a \\ T_M b - T_T \\ -T_M \end{pmatrix}, \tag{2}$$

where $a, b \in \mathbb{R}$ are the longitudinal and lateral main rotor flapping angles; and $T_M, T_T \in \mathbb{R}$ denote the main and tail rotor thrusts. The thrust T_M is positive when the main rotor is generating a force in the $-e'_3$ direction (see Fig. 1). Whereas T_T is defined positive when the tail rotor is generating thrust in the $-e'_2$ direction to compensate the main rotor countertorque. The applied torque can be expressed as

$$\tau = l_T \times \begin{pmatrix} 0 \\ -T_T \\ 0 \end{pmatrix} + l_M \times \begin{pmatrix} -T_M a \\ T_M b \\ -T_M \end{pmatrix} + \begin{pmatrix} 0 \\ -Q_T \\ -Q_M \end{pmatrix}, \tag{3}$$

where $l_M, l_T \in \mathbb{R}^3$ are the positions of the main and tail rotor in $\mathcal{B}$; and $Q_M, Q_T \geq 0$ are the magnitudes of main and tail rotor countertorques.

Next, we make practically reasonable model assumptions to simplify the derivation of a control which compensates SBF. In particular, we consider the tail rotor countertorque to be negligible $Q_T = 0$,

https://doi.org/10.1017/S0263574718000486 Published online by Cambridge University Press

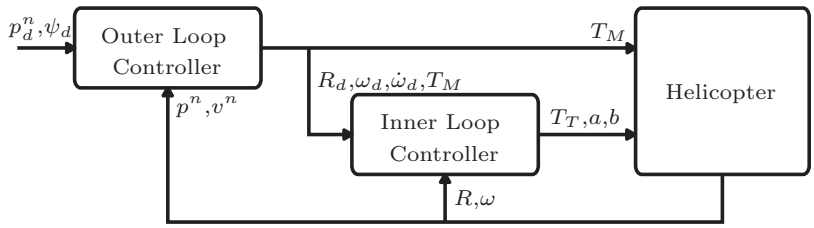


Fig. 2. Block diagram showing the closed-loop system.

the inertia matrix is diagonal $J = \text{diag}(J_x, J_y, J_z)$, and the rotor offsets are $l_M = (0\ 0\ -z_M)^T$ and $l_T = (-x_T\ 0\ 0)^T$. Therefore, (3) simplifies to

$$\tau = \begin{pmatrix} \tau_1 \\ \tau_2 \\ \tau_3 \end{pmatrix} = \begin{pmatrix} z_M T_M b \\ z_M T_M a \\ x_T T_T - Q_M \end{pmatrix}. \tag{4}$$

The relation (4) is a one-to-one mapping from τ to a, b, T_T. Hence, we can use it in (2) to obtain

$$f = R \begin{pmatrix} -\frac{\tau_2}{z_M} \\ \frac{\tau_1}{z_M} - \frac{\tau_3}{x_T} - \frac{Q_M}{x_T} \\ -T_M \end{pmatrix}. \tag{5}$$

From (5), we see the SBF is in part due to the applied torque and in part due to the countertorque. Finally, we assume the main rotor countertorque is linear in the main rotor thrust $Q_M = \sigma_M T_M$ for some constant $\sigma_M > 0$.

The assumptions made in this section are practically reasonable and consistent with current designs in the literature. Indeed, the tail countertorque is not considered in refs. [1, 36], and in ref. [8] similar assumptions are made regarding the rotor hub offsets. Furthermore, based on the geometry of the helicopter it is reasonable to expect that the body frame $\mathcal{B}$ is aligned with the principal axes, and this justifies the diagonal inertia matrix.

3. Control Design

The goal of the controller is to track reference trajectories denoted $p_d^n : \mathbb{R} \to \mathbb{R}^3$ for position, and $\psi_d : \mathbb{R} \to \mathbb{R}$ for heading. We perform the control design using an inner-outer hierarchical approach. As shown in Fig. 2, the inner-loop controls orientation, while the outer-loop controls position. In order to perform the outer-loop design we assume the inner-loop perfectly tracks the orientation reference from the outer-loop. An overview of our approach is as follows. By first designing the inner-loop control we obtain expressions for the rotational inputs. The SBF terms in the outer-loop dynamics can now be considered as known parameters as opposed to inputs. By substituting the inner-loop control into the SBF terms, the control design can proceed in a standard manner by defining an input transformation which compensates for the model in feedforward, and a feedback to stabilize the resulting dynamics.

3.1. Inner-loop control

Control of the rotational dynamics can be performed by applying an existing design from the literature. Our design is based on ref. [23] and its refinement in ref. [5]. This design is chosen since it does not suffer from singularities or other topological constraints due to the choice of parametrization, and it provides almost global asymptotic stability on $SO(3) \times \mathbb{R}^3$. To begin, we define error coordinates $\tilde{R} = R_d^T R$ and $\tilde{\omega} = \omega - \tilde{R}^T \omega_d$, where the subscript ω_d denotes a desired quantity. The open-loop error

https://doi.org/10.1017/S0263574718000486 Published online by Cambridge University Press

dynamics are

$$\dot{\tilde{R}} = \tilde{R}\hat{\tilde{\omega}} \tag{6a}$$

$$J\dot{\tilde{\omega}} = -\omega \times J\tilde{\omega} + \tau - J\tilde{R}^T\dot{\omega}_d + J\hat{\omega}\tilde{R}^T\omega_d. \tag{6b}$$

These dynamics are stabilized using torque feedback

$$\tau = -\operatorname{skew}(K_p^r\tilde{R})^\vee - K_d^r\tilde{\omega} - J\hat{\omega}\tilde{R}^T\omega_d + J\tilde{R}^T\dot{\omega}_d + (\tilde{R}^T\omega_d)^\wedge J\tilde{\omega}, \tag{7}$$

where $K_p^r, K_d^r \in \mathbb{R}^{3\times 3}$ are diagonal, positive definite gain matrices, and $\operatorname{skew}(A) = \frac{1}{2}(A - A^T)$. The closed-loop dynamics become

$$\dot{\tilde{R}} = \tilde{R}\hat{\tilde{\omega}} \tag{8a}$$

$$J\dot{\tilde{\omega}} = -\tilde{\omega} \times J\tilde{\omega} - \operatorname{skew}(K_p^r\tilde{R})^\vee - K_d^r\tilde{\omega}. \tag{8b}$$

We consider $(\tilde{R},\ \tilde{\omega}) = (I, 0)$ which is an equilibrium of (8). About this point

$$V = \frac{1}{2}\operatorname{tr}(K_p^r(I - \tilde{R})) + \frac{1}{2}\tilde{\omega}^T J\tilde{\omega}$$

is a Lyapunov function candidate. Consider

$$V_1 = \frac{1}{2}\operatorname{tr}(K_p^r(I - \tilde{R})). \tag{9}$$

Then

$$\dot{V}_1 = -\frac{1}{2}\operatorname{tr}(K_p^r\dot{\tilde{R}}) = -\frac{1}{2}\operatorname{tr}\left(\left(\operatorname{skew}(K_p^r\tilde{R}) + \operatorname{sym}(K_p^r\tilde{R})\right)\tilde{R}^T\dot{\tilde{R}}\right),$$

where $\operatorname{sym}(A) = \frac{1}{2}(A + A^T)$, and we have used the fact that any matrix can be decomposed as $A = \operatorname{skew}(A) + \operatorname{sym}(A)$.[16] Since symmetric and skew-symmetric matrices are orthogonal under the trace norm, and $\hat{\omega} = \tilde{R}^T\dot{\tilde{R}}$, we have

$$\dot{V}_1 = -\frac{1}{2}\operatorname{tr}\left(\operatorname{skew}(K_p^r\tilde{R})\hat{\omega}\right).$$

Finally, since for $a, b \in \mathbb{R}^3$, $a \cdot b = -\frac{1}{2}\operatorname{tr}(\hat{a}\hat{b})$, we have

$$\dot{V}_1 = \tilde{\omega}^T\operatorname{skew}(K_p^r\tilde{R})^\vee.$$

Using (8) we compute

$$\dot{V} = \operatorname{skew}(K_p^r\tilde{R})^\vee \cdot \tilde{\omega} + \tilde{\omega} \cdot (-\tilde{\omega} \times J\tilde{\omega} - \operatorname{skew}(K_p^r\tilde{R})^\vee - K_d^r\tilde{\omega}) = -\tilde{\omega}^T K_d^r\tilde{\omega}.$$

Therefore, the equilibrium $(\tilde{R},\ \tilde{\omega}) = (I, 0)$ of (8) is asymptotically stable. The stability of $(I, 0)$ is not global since there are at least three other closed-loop equilibria. In particular, when the eigenvalues of K_p^r are distinct the 180° rotations about the coordinate axes are the three remaining equilibria. For further detail see ref. [5].

Although any stabilizing control can be chosen for the inner loop, the particular approach presented here is theoretically elegant since it avoids singularities. In Section 5, we use this approach for simulation. For ease of implementation, we use an industry standard PID inner-loop in Section 6 for the experimental validation.

https://doi.org/10.1017/S0263574718000486 Published online by Cambridge University Press

3.2. Outer-loop control

To design the outer-loop control we will treat the translational dynamics as an independent subsystem forced by the desired roll ϕ_d, pitch θ_d and main rotor thrust T_M. We begin with dynamics (1a) and (1b), where f is taken as the input. These dynamics are essentially three decoupled double integrators, and therefore stabilization is trivial. However, to apply such a control requires its expression in terms of $(\phi_d,\ \theta_d,\ T_M)$. As shown in Section 3.2.1, writing this expression leads to unstable dynamics for $\phi_d,\ \theta_d$. Hence, such a control cannot be implemented.

To illustrate this difficulty with such an approach, we define error states $\tilde{p}^n = p^n - p_d^n$ and $\tilde{v}^n = v^n - \dot{p}_d^n$ which results in the error dynamics

$$\dot{\tilde{p}}^n = \tilde{v}^n \tag{10a}$$

$$m\dot{\tilde{v}}^n = mge_3 - m\ddot{p}_d^n + f. \tag{10b}$$

If we choose the feedback

$$f = m\ddot{p}_d^n - mge_3 - K_d^t\tilde{v}^n - K_p^t\tilde{p}^n, \tag{11}$$

where K_d^t and K_p^t are symmetric positive definite gain matrices, and consider the Lyapunov function candidate

$$V = \frac{m}{2}(\tilde{v}^n)^T\tilde{v}^n + \frac{1}{2}(\tilde{p}^n)^T K_p^t\tilde{p}^n,$$

The derivative of V along the trajectories of (10) is

$$\dot{V} = -(\tilde{v}^n)^T K_d^t\tilde{v}^n$$

which implies the closed-loop translational subsystem is globally asymptotically stable.

3.2.1. Unstable reference dynamics. Next, we derive the differential equations for ϕ_d and θ_d which must be satisfied if the control (11) were to be applied. We deduce the instability of these differential equations from their linearization. Later in Section 3.2.2, we ignore terms in (5) which create the unstable dynamics, but we compensate for the effect of the tail rotor on the translational dynamics. Therefore, the control will compensate for the primary effect of the SBF due to the tail rotor which is present during hover and slow trajectories. In order to isolate ϕ_d and θ_d we define a transformed input

$$\nu = R_{zd}^T f, \tag{12}$$

where f is given in (2). We must now relate the stabilizing force (11) to the outer-loop inputs: ϕ_d, θ_d, and T_M:

$$\nu_1 = s\phi_d s\theta_d\left(\frac{\tau_1}{z_M} - \frac{\tau_3}{x_T} - \frac{Q_M}{x_T}\right) - c\theta_d\frac{\tau_2}{z_M} - T_M c\phi_d s\theta_d \tag{13a}$$

$$\nu_2 = c\phi_d\left(\frac{\tau_1}{z_M} - \frac{\tau_3}{x_T} - \frac{Q_M}{x_T}\right) + s\phi_d T_M \tag{13b}$$

$$\nu_3 = s\theta_d\frac{\tau_2}{z_M} + c\theta_d s\phi_d\left(\frac{\tau_1}{z_M} - \frac{\tau_3}{x_T} - \frac{Q_M}{x_T}\right) - c\phi_d s\phi_d T_M. \tag{13c}$$

Thus, in order to evaluate (13), we require an expression for the applied torque. This expression is found by evaluating (7) when the rotational dynamics are tracking the reference

$$\tau = J\dot{\omega}_d. \tag{14}$$

https://doi.org/10.1017/S0263574718000486 Published online by Cambridge University Press

The angular acceleration $\dot{\omega}_d$ can be expressed in terms of $(\phi_d,\ \theta_d,\ \psi_d)$ using the standard kinematic expression

$$\omega_d = \begin{pmatrix} 1 & 0 & -s\theta_d \\ 0 & c\phi_d & s\phi_d c\theta_d \\ 0 & -s\phi_d & c\phi_d c\theta_d \end{pmatrix} \begin{pmatrix} \dot{\phi}_d \\ \dot{\theta}_d \\ \dot{\psi}_d \end{pmatrix}. \tag{15}$$

We differentiate (15) to obtain

$$\dot{\omega}_d = \begin{pmatrix} 1 & 0 & -s\theta_d \\ 0 & c\phi_d & s\phi_d c\theta_d \\ 0 & -s\phi_d & c\phi_d c\theta_d \end{pmatrix} \begin{pmatrix} \ddot{\phi}_d \\ \ddot{\theta}_d \\ \ddot{\psi}_d \end{pmatrix} + \begin{pmatrix} 0 & 0 & -c\theta_d \\ -s\phi_d & c\phi_d c\theta_d & -s\phi_d s\theta_d \\ -c\phi_d & -s\phi_d c\theta_d & -c\phi_d s\theta_d \end{pmatrix} \begin{pmatrix} \dot{\phi}_d\dot{\theta}_d \\ \dot{\phi}_d\dot{\psi}_d \\ \dot{\theta}_d\dot{\psi}_d \end{pmatrix}. \tag{16}$$

It is these expressions for the components τ which introduce first and second derivatives of the reference orientation into (13).

The linearization of the dynamics for the inputs ϕ_d and θ_d is not asymptotically stable if we consider a constant position and heading reference. Assume the system is initialized on its reference. In other words, $\dot{\psi}_d = \ddot{\psi}_d = \nu_1 = \nu_2 = 0$, and ν_3 is constant. Let $\zeta_1 = \phi_d$, $\zeta_2 = \theta_d$, $\zeta_3 = \dot{\phi}_d$, and $\zeta_4 = \dot{\theta}_d$. Then, the reference dynamics become

$$\dot{\zeta}_1 = \zeta_3 \tag{17a}$$

$$\dot{\zeta}_2 = \zeta_4 \tag{17b}$$

$$\dot{\zeta}_3 = z_M \nu_3 \left(\frac{s\zeta_1 c\zeta_2}{J_x} - \frac{c\zeta_1 c\zeta_2 \sigma_M}{J_x x_T} - \frac{z_M J_z t\zeta_1 s\zeta_2}{J_x J_y x_T} \right) - \frac{z_M J_z \zeta_3 \zeta_4}{J_x x_T} (t\zeta_1 s\zeta_1 + c\zeta_1) \tag{17c}$$

$$\dot{\zeta}_4 = t\zeta_1\zeta_3\zeta_4 + \frac{s\zeta_2 z_M \nu_3}{c\zeta_1 J_y}, \tag{17d}$$

where $s\phi = \sin\phi$, $c\phi = \cos\phi$, and $t\phi = \tan\phi$. The equilibrium of (17) is $\zeta_1 = \arctan\left(\frac{\sigma_M}{x_T}\right)$, $\zeta_2 = \zeta_3 = \zeta_4 = 0$. The eigenvalues of the approximate linearization of (17) are two repeated pairs

$$\lambda = \pm \sqrt{\frac{z_M \sqrt{\sigma_M^2 + x_T^2}}{2 J_x J_y x_T} \left(\nu_3 (J_x + J_y) + |\nu_3 (J_x - J_y)| \right)},$$

where z_M, x_T, J_x, J_y are positive. Thus, the linearization of the dynamics (17) is unstable making it impractical to apply (11).

3.2.2. Main result: Tail rotor SBF compensation. Since we cannot apply a control law based on an unstable reference dynamics, we partition (5) in order to derive an orientation reference. In particular, we treat any terms in f with dependence on derivatives of θ_d or ϕ_d as a disturbance in the design. Effectively, we break f into two terms $f = R_{zd}\nu + R_d\bar{\tau}$ where we have redefined ν and defined a disturbance $\bar{\tau}$. That is,

$$\nu = R_{yd} R_{xd} \begin{pmatrix} 0 \\ -\frac{c\phi_d c\theta_d J_z \ddot{\psi}_d}{x_T} - \frac{\sigma_M T_M}{x_T} \\ -T_M \end{pmatrix} \tag{18}$$

and

$$\bar{\tau} = \begin{pmatrix} -\frac{\tau_2}{z_M} \\ \frac{\tau_1}{z_M} + \frac{J_z}{x_T} \left(s\phi_d \ddot{\theta}_d + c\phi_d \dot{\phi}_d \dot{\theta}_d + s\phi_d c\theta_d \dot{\phi}_d \dot{\psi}_d + c\phi_d s\theta_d \dot{\theta}_d \dot{\psi}_d \right) \\ 0 \end{pmatrix}, \tag{19}$$

where we have used (14)–(16) to express τ as a function of ϕ_d, θ_d, ψ_d, and their derivatives.

https://doi.org/10.1017/S0263574718000486 Published online by Cambridge University Press

We proceed with the design by ignoring $\bar{\tau}$. In other words, we have neglected the effect of the SBF due to the flapping angles as well as the coupling of the roll and pitch into the expression for the tail rotor thrust in the SBF. However, we have retained the principal effect of the SBF due to the tail rotor. Indeed, for many practical trajectories only constant steady-state roll-pitch speeds are required (e.g., hover, constant velocity forward flight, and circles when the heading is tangent to the position trajectory). However, the main rotor countertorque is always present, and $\ddot{\psi}_d$ is used to change the heading at low linear velocity and hover. To complete the control design we expand (18) to get

$$\nu_1 = s\phi_d s\theta_d \left(-\frac{c\phi_d c\theta_d J_z \ddot{\psi}_d}{x_T} - \frac{\sigma_M T_M}{x_T} \right) - c\phi_d s\theta_d T_M$$

$$\nu_2 = c\phi_d \left(-\frac{c\phi_d c\theta_d J_z \ddot{\psi}_d}{x_T} - \frac{\sigma_M T_M}{x_T} \right) + s\phi_d T_M$$

$$\nu_3 = c\theta_d s\phi_d \left(-\frac{c\phi_d c\theta_d J_z \ddot{\psi}_d}{x_T} - \frac{\sigma_M T_M}{x_T} \right) - c\phi_d c\theta_d T_M$$

and solve for T_M, θ_d, ϕ_d to obtain

$$T_M = -\frac{(c\theta_d)^2 s\phi_d c\phi_d J_z \ddot{\psi}_d + \nu_3 x_T}{c\theta_d (s\phi_d \sigma_M + x_T c\phi_d)} \tag{20a}$$

$$\theta_d = \arctan \frac{\nu_1}{\nu_3} \tag{20b}$$

$$\phi_d = \arctan \left(\frac{J_z \ddot{\psi}_d \nu_3 - \sqrt{\nu_1^2 + \nu_3^2} \left(\sigma_M \sqrt{\nu_1^2 + \nu_3^2} + x_T \nu_2 \right)}{\sqrt{\nu_1^2 + \nu_3^2} \left(\sigma_M \nu_2 - x_T \sqrt{\nu_1^2 + \nu_3^2} \right)} \right), \tag{20c}$$

where we have assumed $\nu_3 < 0$. To implement the control using (20) in practice we compute ν from (12) and f from (11). We note that for practically relevant trajectories $|\nu_1| \ll |\nu_3|$ and $|\nu_2| \ll |\nu_3|$ since the force of gravity will be applied mainly in the e_3' direction. Using a similar Lyapunov stability argument as given above (at the beginning of Section 3.2) we have the following proposition.

Proposition 1. *Let p_d^n and ψ_d be the position and heading references, respectively, and the outer-loop subsystem be*

$$\dot{p}^n = v \tag{21a}$$

$$m\dot{v}^n = mge_3 + R_{zd}\nu, \tag{21b}$$

where the inputs are $(\phi_d,\ \theta_d,\ T_M)$ as given by (20)*. Then the control*

$$\nu = R_{zd}^T \left(m\ddot{p}_d^n - mge_3 - K_p^t \tilde{p}^n - K_d^t \tilde{v}^n \right) \tag{22}$$

which is applied using (20)*, will cause* (21) *to track the reference with asymptotically stable error dynamics on the domain where $\nu_3 < 0$.*

Remark 2. The restriction of the state space to the domain where $\nu_3 < 0$ is necessary in order to prevent T_M from crossing zero. If $T_M = 0$ the helicopter becomes uncontrollable, and this is a situation we do not consider here. In practice, for noninverted flight this case is not relevant. Indeed, experimental data we have collected during an investigation of main rotor thrust modelling where the pilot attempted to maximize downward acceleration while retaining control showed T_M is greater than $mg/3$.[12]

https://doi.org/10.1017/S0263574718000486 Published online by Cambridge University Press

4. Robustness Analysis

The purpose of this section is to determine if conditions exist where stability of the outer-loop can be guaranteed in the presence of the disturbance $\bar{\tau}$. We will show that for a general reference the dynamics are uniformly ultimately bounded, and for a constant-velocity, constant-heading reference the result specializes to asymptotic stability. The definition of ultimately bounded is from [22, Definition 4.6]. The undisturbed closed-loop error dynamics are a stable linear system $\dot{\xi} = A\xi$, where $A = \begin{pmatrix} 0 & I \\ -K_p^t & -K_d^t \end{pmatrix}$ and $\xi = \begin{pmatrix} \tilde{p}^n \\ \tilde{v}^n \end{pmatrix}$. Therefore, we know for any symmetric positive definite Q there exists a symmetric positive definite P such that $V = \xi^T P \xi$ is a Lyapunov function with derivative $\dot{V} = -\xi^T Q \xi$. When the effect of $\bar{\tau}$ is included, we have

$$\dot{V} = -\xi^T Q \xi + 2\xi^T P \begin{pmatrix} 0 \\ R_d \bar{\tau} \end{pmatrix}. \tag{23}$$

In (23), we see that the first term is stabilizing while the second is indefinite. Therefore, we seek a comparison of the magnitude of these terms. Let $\lambda_{\min}(M)$ ($\lambda_{\max}(M)$), $M \in \mathbb{R}^{n\times n}$ be the minimum (maximum) eigenvalue of a matrix M, then

$$\dot{V} \leq -\lambda_{\min}(Q)\|\xi\|^2 + 2\lambda_{\max}(P)\|\xi\|\|\bar{\tau}\|. \tag{24}$$

In order to determine whether this inequality can guarantee stability we must compute an upper bound on $\bar{\tau}$ in terms of the magnitude of the error states.

The relationship between $\bar{\tau}$ and the error state ξ is defined by the composition

$$\bar{\tau}(\xi) = \bar{\tau} \circ \dot{\omega}_d \circ \nu \circ f(\xi),$$

where $\bar{\tau}(\dot{\omega}_d)$ is found using $\tau = J\dot{\omega}_d$, $\dot{\omega}_d(\nu)$ is from (20b)–(20c), $\nu(f) = R_{zd}^T f$, and $f(\xi)$ is given by (11). Therefore, to derive a growth bound on $\bar{\tau}$ in terms of $\|\xi\|$ we proceed by deriving a bound on each of these functions. A bound on $\|f\|$ and its first two derivatives is

$$\|f\| \leq m\|\ddot{p}_d^n\| + mg + (\bar{k}_d + \bar{k}_p)\|\xi\| \tag{25a}$$

$$\|\dot{f}\| \leq m\|(p_d^n)^{(3)}\| + (\bar{k}_d^2 + \bar{k}_d\bar{k}_p + \bar{k}_p)\|\xi\| \tag{25b}$$

$$\|\ddot{f}\| \leq m\|(p_d^n)^{(4)}\| + (\bar{k}_d^3 + 2\bar{k}_d\bar{k}_p + \bar{k}_d^2\bar{k}_p + \bar{k}_p^2)\|\xi\|, \tag{25c}$$

where we have assumed K_p^t and K_d^t are diagonal, $\bar{k}_d = \lambda_{\max}(K_d^t)$, and $\bar{k}_p = \lambda_{\max}(K_p^t)$. We have bounded two derivatives since they appear in $\dot{\omega}_d(\nu)$. Next, we have

$$\|\nu\| = \|f\| \tag{26a}$$

$$\|\dot{\nu}\| \leq \|\dot{f}\| + |\dot{\psi}_d|\|f\| \tag{26b}$$

$$\|\ddot{\nu}\| \leq \|\ddot{f}\| + 2|\dot{\psi}_d|\|\dot{f}\| + (|\dot{\psi}_d|^2 + |\ddot{\psi}_d|)\|f\|. \tag{26c}$$

The computation of the growth bounds on the first two derivatives of ϕ_d and θ_d results in long expressions which cannot be presented here. However, it is important to note that they are independent of the upper bound of $|\nu_3|$. Indeed, when a constant-velocity reference is used we see from (25) that the upper bound on $|\nu_3|$ will depend on the constant mg even when the magnitude of the error state is zero. Since the growth of the orientation reference derivatives can be bounded independently of mg, it is possible to show asymptotic stability for a constant-velocity, constant-heading reference. We clarify this idea by computing explicit bounds for this special case. When $\dot{\psi}_d = 0$ then (20c) becomes

$$\phi_d = -\arctan\left(\frac{\sigma_M\sqrt{\nu_1^2 + \nu_3^2} + x_T\nu_2}{\sigma_M\nu_2 - x_T\sqrt{\nu_1^2 + \nu_3^2}}\right).$$

https://doi.org/10.1017/S0263574718000486 Published online by Cambridge University Press

Bounds on the derivatives of ϕ_d are found to be

$$|\dot{\phi}_d| \leq \frac{3\|\dot{\nu}\|}{|\nu_3|} \tag{27a}$$

and

$$|\ddot{\phi}_d| \leq \frac{6\|\dot{\nu}\|^2}{|\nu_3|^3} + \frac{\|\ddot{\nu}\|}{|\nu_3|} + \frac{18\|\dot{\nu}\|}{|\nu_3|^3} + \frac{3\|\dot{\nu}\||\nu_1|}{|\nu_3|^3}. \tag{27b}$$

Remark that (27) is independent of the upper bound of $|\nu_3|$. Instead we are only concerned with a lower bound on $|\nu_3|$. Therefore, there is no constant term in (27) due to the force of gravity. Bounds on the derivatives of θ_d are found by differentiating (20b) to obtain

$$|\dot{\theta}_d| \leq \frac{\|\dot{\nu}\|}{|\nu_3|} + \frac{\|\dot{\nu}\||\nu_1|}{\nu_3^2} \tag{28a}$$

$$|\ddot{\theta}_d| \leq \frac{\|\ddot{\nu}\|}{|\nu_3|} + \frac{\|\ddot{\nu}\||\nu_1|}{\nu_3^2} + \frac{2\|\dot{\nu}\|^2}{\nu_3^2} + \frac{4\|\dot{\nu}\|^2|\nu_1|}{|\nu_3|^3} + \frac{2\|\dot{\nu}\|^2|\nu_1|^2}{\nu_3^4}. \tag{28b}$$

Finally, $\|\bar{\tau}\| \leq \|J\|\,\|\dot{\omega}_d\|$, and hence

$$\|\bar{\tau}\| \leq \sqrt{3}\|J\|\left(|\ddot{\phi}_d| + |\ddot{\theta}_d| + |\ddot{\psi}_d| + |\dot{\phi}_d|^2 + |\dot{\theta}_d|^2 + |\dot{\psi}_d|^2\right). \tag{29}$$

We can now state the main result of our analysis in the following theorem.

Theorem 3. *Let ψ_d be a heading reference and p_d^n be a position reference. If $|\psi_d^{(i)}| \leq l_1$ for $i \geq 1$, $\|(p_d^n)^{(i)}\| \leq l_2$ for $i \geq 2$, and $l = \max\{l_1, l_2\}$, then the dynamics* (10) *with $f = R_{zd}\nu$ and the inputs ϕ_d, θ_d and T_M given by* (20)*, are uniformly ultimately bounded.*

Proof. The bound on $\bar{\tau}$ is found to be of the form $\|\bar{\tau}\| \leq \sum_{n=0}^{10} c_n\|\xi\|^n$. We observe that for any $\rho > 0$ there exists $r > 0$ such that $\sum_{n=2}^{10} c_n\|\xi\|^n < \rho\|\xi\|$ for $\|\xi\| < r$. Therefore, from (24) it follows that

$$\dot{V} \leq -(1 + 2\lambda_{\max}(P)(c_1 + \rho))\|\xi\|^2 + 2\lambda_{\max}(P)c_0\|\xi\|,$$

where $\|\xi\| < r$, and we have chosen $Q = I$ in order to maximize the ratio $\frac{\lambda_{\min}(Q)}{\lambda_{\max}(P)}$.[32] Thus, for

$$\rho \leq \frac{1}{2\lambda_{\max}(P)} - c_1$$

we can conclude uniform ultimate boundedness as long as

$$\frac{2\lambda_{\max}(P)c_0}{1 - 2\lambda_{\max}(P)(c_1 + \rho)} \leq r$$

which can always be satisfied by choosing l sufficiently small since $c_0 = \sum_{n=1}^{12} c_n' l^n$, for some constants $c_n' > 0$. □

Next, we consider the special case of a constant-heading, constant-velocity reference trajectory, which is practically relevant.

Corollary 4. *Let p_d^n be a reference trajectory with constant velocity, and ψ_d be a constant heading reference. Then, the dynamics* (10) *with $f = R_{zd}\nu$ and the inputs ϕ_d, θ_d and T_M given by* (20) *are asymptotically stable.*

https://doi.org/10.1017/S0263574718000486 Published online by Cambridge University Press

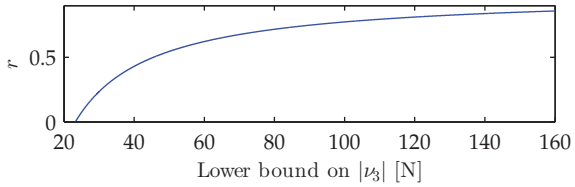


Fig. 3. Relationship between the region of attraction r and the lower bound on $|\nu_3|$ given by (32) for $\bar{k}_d = 0.3$ and $\bar{k}_p = 0.2$.

Proof. Beginning with (29), we derive a growth bound on $\|\bar{\tau}\|$ in terms of $\|\xi\|$ by simplifying (26) and (25) using the given assumptions on the reference trajectory. We obtain the bounds

$$\begin{aligned}
|\nu_1| &\leq (\bar{k}_d + \bar{k}_p)\|\xi\| \\
\|\dot{\nu}\| &\leq (\bar{k}_d^2 + \bar{k}_d\bar{k}_p + \bar{k}_p)\|\xi\| \\
\|\ddot{\nu}\| &\leq (\bar{k}_d^3 + 2\bar{k}_d\bar{k}_p + \bar{k}_d^2\bar{k}_p + \bar{k}_p^2)\|\xi\|
\end{aligned}$$

which we combine with (27) and (28) to obtain

$$\|\bar{\tau}\| \leq \sum_{n=1}^{4} c_n \|\xi\|^n. \tag{30}$$

Thus,

$$\dot{V} \leq -\left(1 - 2\lambda_{\max}(P)(c_1 + \rho)\right)\|\xi\|^2, \quad \text{when } \|\xi\| < r,$$

where $Q = I$. Finally, we can conclude asymptotic stability by choosing

$$\rho \leq \frac{1}{2\lambda_{\max}(P)} - c_1. \tag{31}$$

□

Remark 5. As an alternative to the latter part of the proof, if we restrict our interest to $\|\xi\| < 1$ we can express the growth bound (30) as $\|\bar{\tau}\| \leq \bar{c}\|\xi\| \sum_{n=1}^{3} \|\xi\|^n$, where $\bar{c} = \max\{c_n\}$. Thus,

$$\dot{V} \leq -\left(1 - \frac{2\lambda_{\max}(P)\bar{c}}{1-r}\right)\|\xi\|^2 - \frac{2\lambda_{\max}(P)\bar{c}\|\xi\|^5}{1-r},$$

where $\|\xi\| < r$. This implies asymptotic stability for

$$\frac{1}{2\lambda_{\max}(P)} \geq \frac{\bar{c}}{1-r}. \tag{32}$$

Remark 6. For a particular choice of controller gains, the bounds (31) and (32) provide a design trade-off between r and a lower bound on $|\nu_3|$. A particular numerical example clarifies the relationship. We choose $K_d^t = \bar{k}_d I$ and $K_p^t = \bar{k}_p I$, where $\bar{k}_d = 0.3$ and $\bar{k}_p = 0.2$. We use the value of $\|J\|_2 = 1.48$, $\bar{c} = c_1$, and $c_1 \approx \frac{1.05}{|\nu_3|} + \frac{16.2}{|\nu_3|^3}$. In addition, when $Q = I$, then $\frac{1}{2\lambda_{\max}(P)} \approx 0.0464$. Thus, (32) becomes $r \leq 1 - \frac{22.6}{|\nu_3|} - \frac{350}{|\nu_3|^3}$. Therefore, by increasing the lower bound on $|\nu_3|$ we can increase the region for which stability is ensured. For example, we can achieve stability for $r = \frac{1}{4}$ if we assume $|\nu_3| > 30 \approx \frac{mg}{5}$. Figure 3 shows this relationship over a range of lower bounds on $|\nu_3|$.

https://doi.org/10.1017/S0263574718000486 Published online by Cambridge University Press

5. Simulation Results

We perform a simulation study to compare a control with and without SBF compensation. As opposed to the experimental results given in Section 6, simulation allows us to isolate the effect of the SBF and more clearly illustrate the benefit of compensating SBF. Therefore, we do not attempt to emulate the experimental environment and neglect effects such as sensor noise and wind. The system is simulated using the dynamics (1) including the SBF (2), where $Q_M = \sigma_M T_M$ in the torque expression (3). The outer-loop control is (20) where ν is from (12) and f is given by (11). The inner-loop control is computed using (7) which is related to the inputs using (4). In the following, we refer to this design as the SBF control. The SBF controller gains used for simulation were $K_p^r = \text{diag}(20,\ 16,\ 30)\ \text{s}^{-2}$, $K_d^r = \text{diag}(7,\ 7,\ 6)\ \text{s}^{-1}$, $K_p^t = 6I$ kg/s, and $K_d^t = 11I$ kg/s^2. For comparison we also simulated a simplified version of the PID-based control described in ref. [13]. Instead of relying entirely on the error feedback, this design compensates the most significant terms in the model. In particular, the rotational control accounts for inertia, principle components of the thrust lever-arms, and the torque from the main rotor. The translational control accounts for the effect of gravity assuming the system is close to hover ($T_M \approx mg$). Using this approach provides a better comparison than a simple application of a PD controller. Since the SBF controller also benefits from these feedforward terms, using a model-based PD control reduces the difference between the two aproaches and better isolates the effect under study. Additionally, compared to ref. [13] the integrators are omitted. Using only the PD terms also improves the comparison to the SBF control. We briefly summarize this design here for the reader's convenience. The rotational control is

$$\begin{pmatrix} a \\ b \\ T_M \end{pmatrix} = \Lambda^r(\ddot{\eta}_d - K_d^r\dot{\tilde{\eta}} - K_p^r\tilde{\eta}) + \begin{pmatrix} 0 \\ 0 \\ \frac{Q_M}{x_T} \end{pmatrix}, \tag{33}$$

where

$$\Lambda^r = \begin{pmatrix} 0 & \frac{J_y}{z_M T_M} & 0 \\ \frac{J_x}{z_M T_M} & 0 & 0 \\ 0 & 0 & \frac{J_z}{x_T} \end{pmatrix},$$

$\eta = (\phi,\ \theta,\ \psi)^T$, $\tilde{\eta} = \eta - \eta_d$, and K_d^r, K_p^r are gain matrices. The translational control is given by

$$\begin{pmatrix} \phi_d \\ \theta_d \\ T_M \end{pmatrix} = \Lambda^t(m\ddot{p}_d^b - K_d^t\tilde{v}^b - K_p^t\tilde{p}^b) + \begin{pmatrix} 0 \\ 0 \\ mg \end{pmatrix},$$

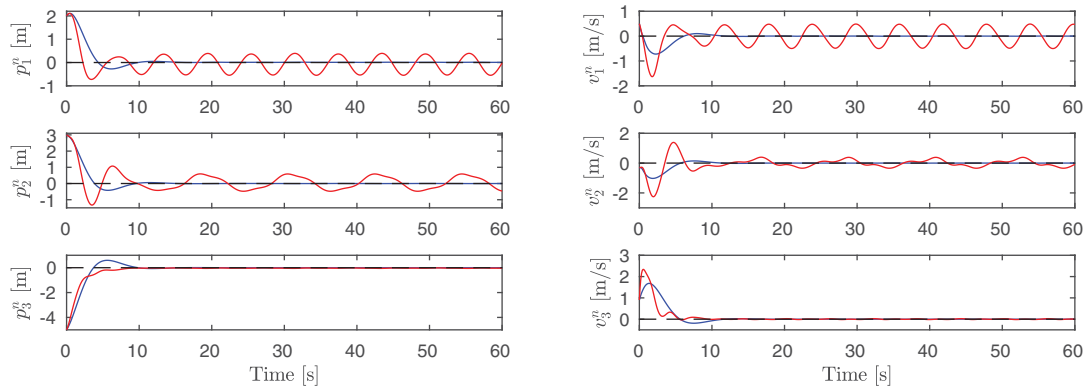
where

$$\Lambda^t = \begin{pmatrix} 0 & \frac{1}{g} & 0 \\ -\frac{1}{g} & 0 & 0 \\ 0 & 0 & -m \end{pmatrix},$$

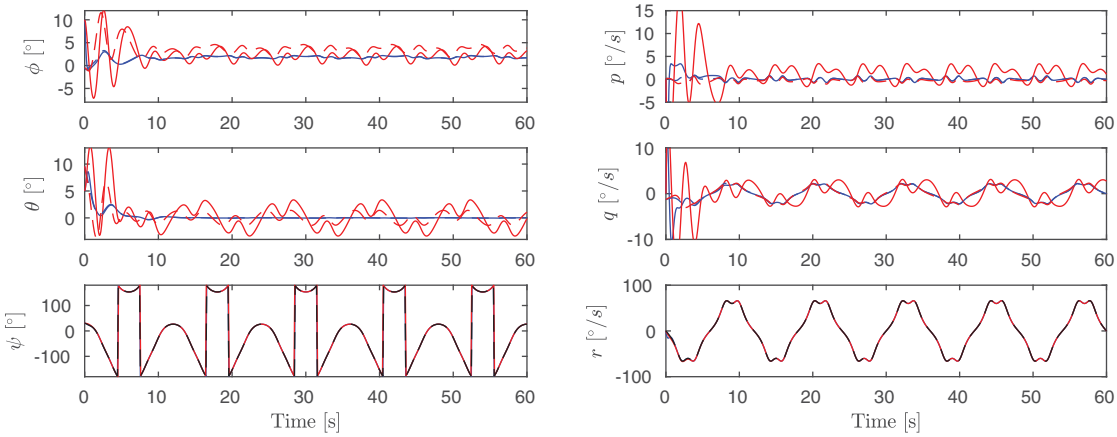
the superscript $\cdot^b$ denotes quantities in $\mathcal{B}$, and K_d^t, K_p^t are gain matrices. The PD controller gains used for simulation are $K_p^r = \text{diag}(10,\ 10,\ 7)\ \text{s}^{-2}$, $K_d^r = 5I\ \text{s}^{-1}$, $K_p^t = 2I\ \text{s}^{-2}$, and $K_d^t = 3I\ \text{s}^{-1}$. The tuning parameters were chosen to provide a similar transient in the position response as seen in Fig. 4(a). The initial conditions are $p_0 = (2,\ 3,\ -5)^T$ m, $v_0 = (0.5,\ -0.3,\ 0.9)^T$ m/s, $\eta_0 = (10^\circ,\ 5^\circ,\ 30^\circ)^T$, $\omega_0 = 0$. These conditions were chosen to give the reader a sense of the transient response of the controllers; however, the steady-state behaviour is the focus of the simulation.

Figure 4 shows the response for a hover simulation. The position reference p_d^n is constant at the origin, and the heading reference ψ_d is time-varying. The heading is commanded to perform alternating

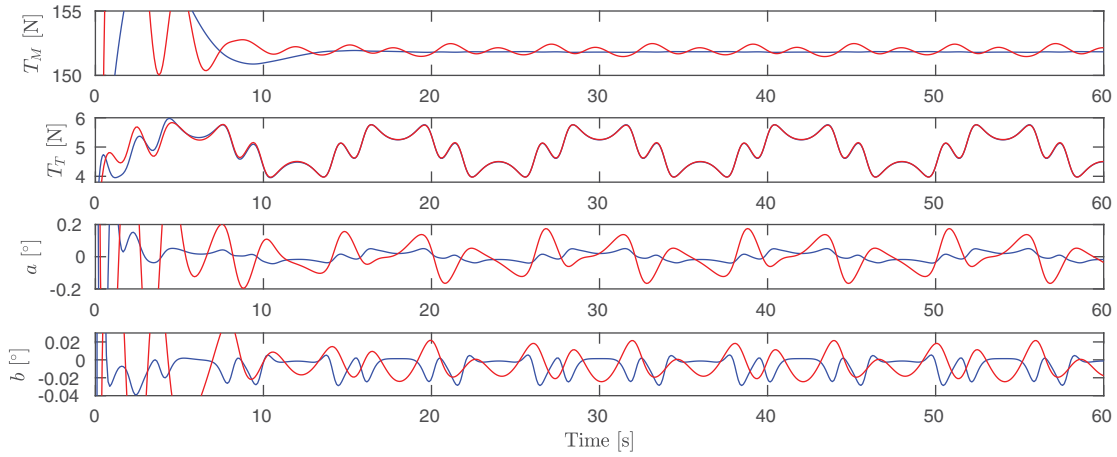
https://doi.org/10.1017/S0263574718000486 Published online by Cambridge University Press



(a) Translational states showing the difference in the response when the tail rotor is compensated. The PD control (shown in red) is not able to converge in the presence of the disturbance, whereas, the SBF-compensated control (shown in blue) converges to the reference.



(b) Rotational states showing the performance improvement using the SBF-compensation. The reference for roll, pitch and respective rates is generated by the outer-loop and is therefore different between the controllers. The PD response is shown in red and its reference is a dashed red line, the SBF-compensated design is shown in blue and its reference is dashed blue.



(c) Control effort for the SBF-compensated control is shown in blue and the PD control in red. Both approaches provide good tracking in yaw, therefore, the tail thrust converges to the same signal. The steady-state behaviour of the flapping angles illustrates the principle difference between the controllers.

Fig. 4. Simulated system response comparing the SBF-compensated control to a classical PD approach. The reference trajectory is a constant position (at the origin) with alternating rotations in yaw.

rotations defined by

$$\psi_d = \arctan\left(\frac{\cos\left(\frac{4\pi}{T_0}t\right)}{2\cos\left(\frac{2\pi}{T_0}t\right)}\right), \tag{34}$$

https://doi.org/10.1017/S0263574718000486 Published online by Cambridge University Press



Fig. 5. ANCL helicopter in flight at Bergen R/C in Cassopolis, MI, October 12, 2012.

where the period $T_0 = 12$ s. This reference trajectory can be seen in Fig. 4(b). It was chosen because it requires a time-varying tail thrust to maintain tracking. This thrust is shown in Fig. 4(c). Since a time-varying tail thrust disturbs the translational dynamics (due to the SBF) as in (5), the PD control has a time-varying error signal and cannot converge to the setpoint. The time-varying disturbance would also prevent an integrator from obtaining convergence if it were included in the controller. However, the SBF control accounts for the disturbance created by the tail thrust and is able to regulate the origin despite its presence. The difference in the response is evident in the horizontal position and velocity shown in the top plots of Fig. 4(a). The presence of the time-varying tail thrust causes the PD control to show steady-state oscillation about the origin. We remark that the amplitude of this oscillation can be reduced by increasing gains; however, it cannot be *eliminated* since it will always appear in the position error as a disturbance. Additionally, in practice it is not usually possible to increase gains arbitrarily. Indeed, large gains lead to actuator saturation and reduced stability margin.

6. Experimental Results

In order to fully validate the design, the control was tested in the field using the Applied Nonlinear Control Lab (ANCL) helicopter shown in Fig. 5. The airframe is a Bergen R/C Industrial Twin helicopter. The avionics include an Ampro Readyboard 800 embedded computer, a Microstrain 3DM-GX3-45 inertial measurement unit (GX3), a Novatel OEM4 DGPS, and a Microhard VIP2400 radio modem. The VIP2400 provides an ethernet link between the onboard computer and the ground station laptop, and it provides an RS-232 connection between the DGPS receivers. The ability to switch between computer control and manual pilot control is provided by the Microbotics SSA20024. The SSA20024 interfaces with the receiver and the servos using a custom-built PCB. The QNX real-time operating system is used to execute the autopilot software. The GPS position and velocity measurements are provided to the GX3 which combines these measurements with its inertial sensor measurements using a Kalman filter and returns an estimate of the full vehicle state. The autopilot software requests the rotational state estimates from the GX3 at 100 Hz and the translational state estimates at 20 Hz. The DGPS measurement is provided to the GX3 at 4 Hz. The control loop is computed at 100 Hz and the control is output at 50 Hz, which is the maximum rate of the SSA20024. Computing the control at a higher frequency than the servo commands reduces the latency caused by generating the servo commands asynchronously to the control calculation. A customized version of the QGroundControl[35] ground station software is used on a Panasonic Toughbook CF-53 running Linux. For further information regarding the platform development see ref. [14]. The nominal values of the helicopter model's physical parameters used in this paper are shown in Table I. For modelling and identification details, see ref. [12].

https://doi.org/10.1017/S0263574718000486 Published online by Cambridge University Press

Table I. Nominal values for the ANCL helicopter's physical parameters.

J_x	0.36	kg m^2
J_y	1.48	kg m^2
J_z	1.21	kg m^2
m	15.5	kg
z_M	0.32	m
x_T	1.06	m
k_p	0.10	rad
k_r	0.013	rad
σ_M	0.04	m

Developing the hardware platform is a significant investment and at the time these results were collected only the ability to control the cyclic inputs had been implemented. Therefore, the autopilot was programmed to control the cyclic inputs while the pilot controlled the main and tail rotor thrusts. Since the focus of this work is the outer-loop control, we used the previously tested[13] inner-loop PID control based on (33) for the attitude. Indeed, by using the existing attitude control we reduced the risks associated with making software changes to a flight control computer (e.g., software errors). Also, additional flight testing is required to tune a new controller. This control has the same structure as the inner-loop used for the PD control in (33) and is given by

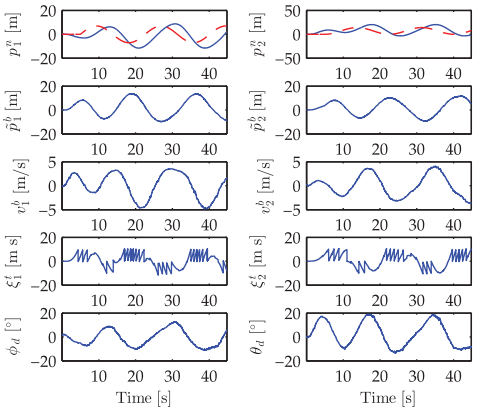
$$\begin{pmatrix} \delta_r \\ \delta_p \end{pmatrix} = -\bar{K}_d^r \underline{\dot{\eta}} - \bar{K}_p^r \underline{\tilde{\eta}} - \bar{K}_i^r \underline{\xi}^r, \tag{35}$$

where the underline denotes that we only use the first two components of the error states; δ_r, δ_p are the normalized roll and pitch servo inputs; and the main rotor torque does not appear since it only affects the yaw dynamics which are not being controlled in this case. The gains in (35) are related to those in (33) by $\bar{K}_j^r = \frac{1}{z_M mg}\begin{pmatrix} \frac{J_x}{k_r} & 0 \\ 0 & \frac{J_y}{k_p} \end{pmatrix} K_j^r$, $j \in \{d, p, i\}$, where k_r, k_p are identified scale factors between the flapping angles and normalized servo inputs. The values of the gains were $\bar{K}_d^r = 0.3I$ s/rad, $\bar{K}_p^r = 0.8I$ rad^{-1}, $\bar{K}_i^r = 0.1I$ rad^{-1}s^{-1}. For the outer-loop control we compute ϕ_d and θ_d as in (20c) and (20b). Since the heading of the vehicle is under manual control we chose to fly with a constant heading to reduce the pilot workload. In this case the derivatives of the heading reference $\dot{\psi}_d$, $\ddot{\psi}_d$ are zero, and this simplifies (20c) while remaining an exact implementation of the design. This simplification is not necessary for implementation and in general time derivatives of the heading reference will be known and can be included. Instead of (22) we compute ν using

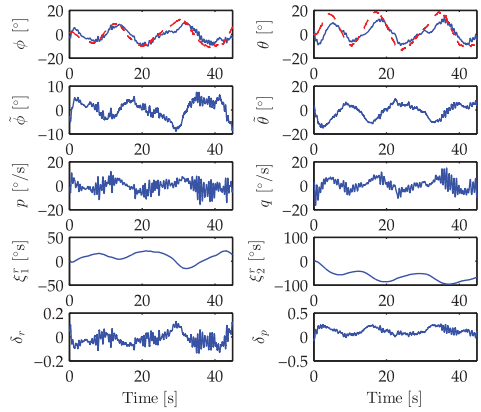
$$\nu = R_z^T \left(-mge_3 - K_d^t v^n - K_p^t \tilde{p}^n - K_i^t \xi^t\right), \tag{36}$$

where the integrator state ξ^t is added for robustness. In addition, we assume the pilot maintains the reference altitude and therefore $\nu_3 = -mg$. Furthermore, the dimension of the gain matrices is reduced to 2×2. The values for the control gains are $K_d^t = 0.22I$ kg/s, $K_p^t = 0.5I$ kg/s^2, $K_i^t = 0.009$ kg/s^3. Remark that in both (35) and (36) we feed back the velocity instead of an error. This difference arises from the design decision to simplify the implementation by avoiding the computation of complex derivative expressions. Indeed, by using a simpler control in practice it was expected that the implementation would be less error-prone. Figure 6 shows the results for tracking a circular trajectory with a 7 m radius and a tangential speed of 2.5 m/s. This trajectory was chosen because when the heading is held constant the SBF are time-varying, and this prevents a PID controller from compensating these forces. This is similar to the figure-8 reference considered in Section 5. During this flight there was a 25 km/h wind coming from the north-west with strong gusts. Given this wind condition, good tracking performance is shown in Fig. 6(c). In order to prevent the controller states from becoming unbounded, the integrators are programmed to reset (return to zero) when an upper bound is reached. The bounds are $|\xi_j^r| \leq 10$ rad s and $|\xi_j^t| \leq 10$ m s where $j \in \{1, 2\}$ denotes the component. The effect of this reset is evident in Fig. 6(a). It is possible that translational tracking

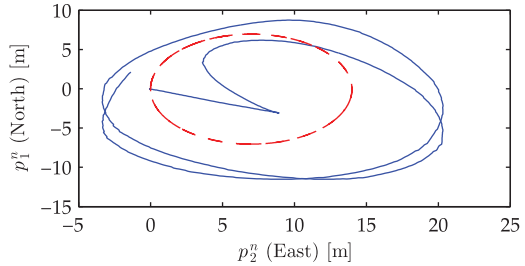
https://doi.org/10.1017/S0263574718000486 Published online by Cambridge University Press



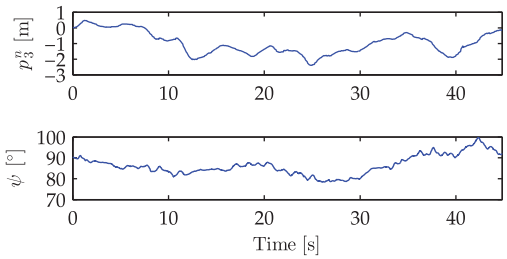
(a) Translational states, errors, and control effort. The reference is shown by the dashed line.



(b) Rotational states, errors and control effort. The reference is shown by the dashed line.



(c) Parametric plot of the horizontal NED position. The reference is shown by the dashed line.



(d) Heading and height measurements.

Fig. 6. System response for circle tracking experiment with a 7 m radius a tangential speed of 2.5 m/s.

error resulted from the ultimate boundedness performance limitation of the control method. Results for PID control were also collected for this trajectory and can be found in ref. [10]. However, a comparison is difficult due to variation in environmental conditions (e.g., effects of wind gusts).

7. Conclusions

The generally accepted model for small unmanned helicopters includes a disturbance to the translational dynamics by the inputs to the rotational dynamics. This disturbance is called the SBF. Despite its inclusion in the model, existing work neglects SBF in control design. This paper has provided a design that compensates the contribution of the tail rotor to the SBF. The approach is based on an inner-outer hierarchical control structure. We present a robustness analysis to the components of SBF which are not directly compensated. The analysis indicates that tracking error will be uniformly ultimately bounded for general reference trajectories. The specific statement of the disturbance bounds given in the robustness analysis provides insight into performance tradeoffs of the design. In the practically relevant special case where the reference has a constant heading and constant velocity (e.g., hover), the position tracking error is asymptotically stable. The design presented in this paper was validated by simulation and in flight tests. The simulation results show our design has performance benefits over a classical PID solution for a hover trajectory with time-varying yaw reference. The steady-state tracking error for the SBF control was negligible, whereas the tracking error for the PID control exhibited large oscillation. In experiment the SBF control yielded bounded tracking error and demonstrated robustness to unmodelled effects such as wind gusts.

References

1. B. Ahmed, H. R. Pota and M. Garratt, "Flight control of a rotary wing UAV using backstepping," *Int. J. Robust Nonlinear Control* **20**, 639–658 (2010).
2. M. Barczyk, Nonlinear State Estimation and Modeling of a Helicopter UAV. *Ph.D. Thesis* (Dept. of Electrical and Computer Engineering, University of Alberta, Edmonton, AB, 2012).

https://doi.org/10.1017/S0263574718000486 Published online by Cambridge University Press

3. M. Bisgaard, Modeling, Estimation, and Control of Helicopter Slung Load System. *Ph.D. Thesis* (Dept. of Control Engineering, Aalborg University, Denmark, 2007).
4. S. Bouabdallah, Design and Control of Quadrotors with Application to Autonomous Flying. *Ph.D. Thesis* (École Polytechnique Federale de Luasanne, Lausanne, Switzerland, 2007).
5. F. Bullo and R. M. Murray, "Tracking for fully actuated mechanical systems: A geometric framework," *Automatica* **35**, 17–35 (1999).
6. D. Cabecinhas, R. Cunha and C. Silverstre, "A nonlinear quadrotor trajectory tracking controller with disturbance rejection," *Control Eng. Practice* **26**, 1–10 (2014).
7. G. Cai, B. M. Chen and T. H. Lee, "Unmanned Rotorcraft Systems," **In**: *Advances in Industrial Control* (Springer-Verlag, London, UK, 2011).
8. P. Castillo, R. Lozano and A. E. Dzul, *Modelling and Control of Mini-Flying Machines* (Springer-Verlag, London, UK, 2005).
9. J. A. Farrell, *Aided Navigation: GPS with High Rate Sensors* (McGraw-Hill, New York, NY, 2008).
10. B. Godbolt, Experimental Nonlinear Control of a Helicopter Unmanned Aerial Vehicle (UAV). *Ph.D. Thesis* (Dept. of Electrical and Computer Engineering, University of Alberta, Edmonton, AB, 2013).
11. B. Godbolt and A. F. Lynch, "A Novel Cascade Controller for a Helicopter UAV with Small Body Force Compensation," *Proceedings of the American Control Conference*, Washington, DC (2013) pp. 800–805.
12. B. Godbolt and A. F. Lynch, "Physical Input Modelling and Identification for a Helicopter UAV," *Proceedings of the International Conference on Unmanned Aircraft Systems*, Atlanta, GA (2013) pp. 890–896.
13. B. Godbolt, N. Vitzilaios, C. Bergen and A. F. Lynch, "Helicopter UAV Control Validation Using Simulation and Experiment," *Proceedings of the International Conference on Unmanned Aircraft Systems*, Atlanta, GA (2013) pp. 392–397.
14. B. Godbolt, N. I. Vitzilaios and A. F. Lynch, "Experimental validation of a helicopter autopilot design using model-based PID control," *J. Intell. Robot. Syst.* **70**, 385–399 (2013).
15. Y. He, H. Pei and T. Sun, "Robust tracking control of helicopters using backstepping with disturbance observers," *Asian J. Control* **16**(5), 1387–1402 (2014).
16. K. Hoffman and R. Kunze, *Linear Algebra*, 2nd ed. (Prentice Hall, Upper Saddle River, NJ, 1971).
17. M. D. Hua, Contributions to the Automatic Control of Aerial Vehicles. *Ph.D. Thesis* (École Doctorale Science et Technologies de l'Information et de la Communication, Université Nice Sophia Antipolis, Nice, France, 2009).
18. M.-D. Hua, T. Hamel, P. Morin and C. Samson, "Introduction to feedback control of underactuated VTOL vehicles: A review of basic control design ideas and principles," *Control Syst. Mag.* **33**, 61–75 (2013).
19. W. Johnson, *Helicopter Theory* (Dover, New York, NY, 1980).
20. S. Kannan, Adaptive Control of Systems in Cascade with Saturation. *Ph.D. Thesis* (School of Aerospace Engineering, Georgia Institute of Technology, Atlanta, GA, 2005).
21. F. Kendoul, I. Fantoni and R. Lozano, "Asymptotic Stability of Hierarchical Inner-Outer Loop-Based Flight Controllers," *Proceedings of the IFAC World Congress*, Seoul, Korea (2008) pp. 1741–1746.
22. H. K. Khalil, *Nonlinear Systems*, 3rd ed. (Prentice Hall, Upper Saddle River, NJ, 2002).
23. D. E. Koditschek, Application of a New Lyapunov Function to Global Adaptive Attitude Tracking," *Proceedings of the Conference on Decision and Control*, Austin, TX (1988) pp. 63–68.
24. T. J. Koo and S. Sastry, "Output Tracking Control Design of a Helicopter Model Based on Approximate Linearization," *Proceedings of the Conference on Decision and Control*, Tampa, FL (1998) pp. 3635–3640.
25. J. G. Leishman, *Principles of Helicopter Aerodynamics* (Cambridge University Press, Cambridge, UK, 2016).
26. R. Mahony and T. Hamel, "Robust trajectory tracking for a scale model autonomous helicopter," *Int. J. Robust Nonlinear Control* **14**, 1035–1059 (2004).
27. P. Marantos, C. P. Bechlioulis and K. J. Kyriakopoulos, "Robust trajectory tracking control for small-scale unmanned helicopters with model uncertainties," *IEEE Trans. Control Syst. Technol.* **25**, 2010–2021 (2017).
28. L. Marconi and R. Naldi, "Robust full degree-of-freedom tracking control of a helicopter," *Automatica* **43**, 1909–1920 (2007).
29. B. Mettler, *Identification Modeling and Characteristics of Miniature Rotorcraft* (Kluwer Academic Publishers, Norwell, MA, 2003).
30. S. Omari, M.-D. Hua, G. Ducard and T. Hamel, "Nonlinear Control of VTOL UAVs Incorporating Flapping Dynamics," *Proceedings of the IEEE/RSJ International Conference on Intelligent Robots and Systems*, Tokyo, Japan (2013) pp. 2419–2425.
31. G. D. Padfield, *Helicopter Flight Dynamics: The Theory and Application of Flying Qualities and Simulation Modeling* (John Wiley & Sons, New York, NY, 2008).
32. R. V. Patel and M. Toda, "Quantitative Measures of Robustness for Multivariable Systems," *Proceedings of the Joint Automatic Control Conference*, San Fransisco, CA (1980). paper TP8-A.
33. R. W. Prouty, *Helicopter Performance, Stability, and Control* (Krieger Publishing Company, Malabar, FL, 1986).
34. px4. PX4 autopilot. Online, 2018. URL `http://pixhawk.org`. Accessed Feb. 27, 2018.
35. QGroundControl. QGroundControl. online, 2013. URL `http://qgroundcontrol.org`. Accessed Feb. 27, 2018.

https://doi.org/10.1017/S0263574718000486 Published online by Cambridge University Press

36. I. A. Raptis, K. P. Valavanis and W. A. Moreno, "A novel nonlinear backstepping controller design for helicopters using the rotation matrix," *IEEE Trans. Control Syst. Technol.* **19**, 465–473 (2011).
37. X. Shao, J. Liu, H. Cao, C. Shen and H. Wang, "Robust dynamic surface trajectory tracking control for a quadrotor UAV via extended state observer," *Int. J. Robust Nonlinear Control* **28**, 2700–2719 (2018).
38. M. D. Shuster, "A survey of attitude representations," *J. Astronaut. Sci.* **41**, 439–517 (1993).
39. K. Valavanis and G. J. Vachtsevanos, eds., *Handbook of Unmanned Aerial Vehicles* (Springer-Verlag, Dordrecht, The Netherlands, 2015).
40. M. J. van Nieuwstadt and R. M. Murray, "Outer Flatness: Trajectory Generation for a Model Helicopter," *Proceedings of the European Control Conference*, Brussels, Belgium (1997) pp. 325–330.
41. B. Xian, B. Zhao, Y. Zhang and X. Zhang, "A low-cost hardware-in-the-loop-simulation testbed of quadrotor UAV and implementation of nonlinear control schemes," *Robotica* **35**, 588–612 (2015).

https://doi.org/10.1017/S0263574718000486 Published online by Cambridge University Press